PAPER

Check for updates

Oxygen vacancy and doping atom effect on electronic structure and optical properties of Cd$_2$SnO$_4$

Mei Tang, [ID] [ab] JiaXiang Shang[a] and Yue Zhang*[a]

The electronic structure and optical properties of oxygen vacancy and La-doped Cd$_2$SnO$_4$ were calculated using the plane-wave-based pseudopotential method based on the density functional theory (DFT) within the generalized gradient approximation (GGA). The formation energy of different oxygen vacancies showed that the V$_{O2}$ oxygen vacancy was easy to obtain in experiments. The Bader charge analysis is implemented to directly observe the electron transfer and distribution for each atom. The calculated band structures show that when the oxygen vacancy was introduced, the impurity energy level appeared in the band gap. The impurity levels induced by oxygen vacancies were mainly composed of O 2p orbits and a very small amount of Cd 4s orbits. After La doping based on the V$_{O2}$ oxygen vacancy of Cd$_2$SnO$_4$, the Fermi energy level entered the conduction band and overlapped with the conduction band which increased the conductivity, and the band gap value increased to above 3.0 eV. The optical calculation results showed that the transmittance of the V$_{O2}$ oxygen vacancy of Cd$_2$SnO$_4$ increased in short wavelength (<600 nm), the reflectivity increased in the infrared region compared with Cd$_2$SnO$_4$, and the transmittance increased to 90% in visible light region after La doping.

I. Introduction

Cadmium stannate (CTO), first discovered in 1960 by Smith, is an important transparent conductive material with great potential to be applied in thin film solar cells and other devices that require low resistance transparent conductive films.[1–3] After grinding cadmium carbonate and tin oxide powder, the powder was sintered at high temperature, and the obtained cadmium stannate powder was determined by X-ray diffraction measurement. The Cd$_2$SnO$_4$ was light yellow and had an orthorhombic crystal structure, and the crystal lattice constant was also listed by Smith.[4] Since then, researchers in the 1960s studied Cd$_2$SnO$_4$, and Smith's work was repeated. In 1972, a Cd$_2$SnO$_4$ film was prepared by radioactive magnetron sputtering of a cadmium stannate ceramic target for the first time by Nozik.[5] The sputtering atmosphere was mixed with argon and argon–oxygen atmosphere, and the film was annealed at low temperature for a long time. The optical bandgap and mobility of the film were measured to obtain a conductivity of $1.33 \times 10^3 \ \Omega^{-1} \ cm^{-1}$. In 2000, after the use of CTO films for CdTe solar cells, Cd$_2$SnO$_4$ was gaining wide attention.[6] In 2001, Wu used CTO thin film as the transparent electrode of CdTe solar cells, and obtained 16.5% solar cell photoelectric conversion efficiency, the world's highest from CdTe.[7]

A variety of methods for preparing the Cd$_2$SnO$_4$ film were then attempted, including chemical vapor deposition (CVD) method,[8] pulsed laser deposition (PLD) method,[9] spray pyrolysis method,[10] sol–gel method,[11,12] electron beam evaporation method,[13] DC sputtering[14–17] and RF sputtering.[18–21] In many of the preparation methods, the CTO films prepared by magnetron sputtering had the lowest resistivity, and the resistivity of films prepared by various magnetron sputtering methods was much lower compared with other methods. In all experiments using magnetron sputtering to deposit CTO thin films, we found that most of the deposited films were heat treated,[22–24] and when the deposition atmosphere contained oxygen, the CTO film can be a low resistance film after heat treatment. The resistivity of the film deposited in the oxygen-containing atmosphere was higher, and the resistivity of the film after annealing in rare gas and reducing hydrogen was lower, and the resistivity of the film was higher after annealing in an oxygen-containing atmosphere. The resistivity of the films deposited in the argon atmosphere was low, but the resistivity results of different films obtained by different researchers after annealing in different atmospheres were different.

However, there were only a few detailed studies of the conductive mechanism of oxygen vacancy of the CTO thin films in the literature.[25] For example, Stapiński *et al.*[26] prepared Cd$_2$SnO$_4$ thin films by DC reactive sputtering, analyzed the types of carriers in the films, it is considered that the carriers in the Cd$_2$SnO$_4$ film was oxygen vacancy or cadmium gap atom. But, oxygen vacancies or cadmium gap atoms provided more

[a]School of Materials Science and Engineering, Beihang University, Beijing 100191, China. E-mail: zhangy@buaa.edu.cn

[b]Journal Publishing Center of Tsinghua University Press, Beijing 100084, China

carriers that had not been studied. It had been suggested that cadmium atoms were occupied by tin atoms, which were also sources of carriers.[27] Ion doping is a method to improve the optical absorption characteristics of materials by introducing different impurity ions, controlling the micro crystal structure and changing the band structure. The rare earth elements possess many special photoelectric properties because of their incomplete occupied 4f electron orbits and empty 5d electron orbits, with rich electronic energy levels and long-lived excited states. They have become one of the new hotspots in the study of wide band gap semiconductor doping systems. By far, there have been no reports on La-doped Cd_2SnO_4 in experiments, and no profound theoretical calculation has been performed on the electronic structure and optical properties of Cd_2SnO_4 in compliance with the density function theory (DFT). In this study, we mainly calculated the effect of oxygen vacancy and doping atoms on the electronic and optical properties of CTO, and the obtained results can provide guidance for preparing Cd_2SnO_4 with high transparent conductive performance.

II.   Calculation methods

The formation energy, electronic structure characteristics and optical properties were calculated by using the pseudopotential plane wave based on the density functional theory (DFT) incorporated in the VASP.[28,29] The exchange and correlation energy was approximated by generalized gradient approximation (GGA).[30] The valence electrons that make up the atoms were processed by the projector augment wave (PAW) scheme.[31] Using the special k point generated by the Monk-horst Pack method,[32] the integral of the reciprocal lattice space was calculated. In order to overcome the band gap underestimation drawback of density function theory calculation, the calculation adopted the first-principle calculation with GGA+U method.[33] Through a series of tests, an effective U_{eff} of 10, 9 and 8 eV was applied for Cd, Sn and O, which were adjusted to reach an agreement with the experimental band gap data.[34] The plane wave cutoff energy is 500 eV and the Monkhorst–Pack k-point sampling is $10 \times 6 \times 3$ for conventional cell of the Cd_2SnO_4.

III.   Results and discussion

A.   The formation energy

Cd_2SnO_4 possesses a space group of Pbam (No. 55) and an orthorhombic structure.[35] The experimental lattice parameters of Cd_2SnO_4 are as follows: $\alpha = \beta = \gamma = 90°$, $a = 3.24937$, $b = 5.66477$, $c = 10.12710$, and the relaxed lattice parameters of pure Cd_2SnO_4 are $a = 3.24928$, $b = 5.66404$, $c = 10.12371$, which are close to the experimental values. There are two oxygen sites in single Cd_2SnO_4 unit cell labeled as O1 and O2. V_{O1} and V_{O2} indicate the case where the different site oxygen atom is removed to form an oxygen vacancy. The $2 \times 2 \times 1$ supercell containing V_{O1} and V_{O2} oxygen vacancy of Cd_2SnO_4 are built, using the $5 \times 5 \times 5$ k-points optimized structure. The convergence standard is set as the force on all atoms being less than 0.01 eV Å^{-1}. The optimized structure is used for the subsequent electronic structure and optical properties calculations.

The formation energy of V_{O1} and V_{O2} models is calculated according to the formula:

$$E_f = E_{defect} - E_{perfect} + \mu_O.$$

Here, E_{defect} and $E_{perfect}$ are the total free energies of the Cd_2SnO_4 without and with V_O. For oxygen-rich environments, μ_O is chemical potential of O, which is determined by the energy of oxygen molecule, $\mu_O = \mu(O_2)/2$.[36] For oxygen-poor conditions, the chemical potential of oxygen atom is determined by $3\mu_O + 2\mu_{La} = \mu(La_2O_3)$. The formation energy values of V_{O1} and V_{O2} oxygen vacancy both in oxygen-rich and oxygen-poor conditions were 3.386, 3.024 eV and -1.20, -1.56 eV. The V_{O2} model formation energy was lower than that of V_{O1} model, indicating that the V_{O2} oxygen vacancy has more stable energetic configuration with local lattice relaxation, so we chose V_{O2} oxygen vacancy in the next calculation. For V_{O2} oxygen vacancy of Cd_2SnO_4 supercell, the structure of La-doped Cd_2SnO_4 was modeled by replacing one Cd atom with one La atom, and the supercell models were in Fig. 1.

The La doping in Cd_2SnO_4 has been considered in different cases, including Cd-substituted (La_{Cd}) and charge-compensated complex $4La_{Cd}3V_{Sn}$ (where V is denoted as vacancy). The calculated formation energies are 8.39, 1.58 and -3.97 eV for La_{Cd} in charge states +1, +2, +3, respectively. The formation energy decreases as the entity charge state increases. The negative value means that La_{Cd}^{3+} formation is more energetically favorable than the other native point defects formed in the host lattice. Clearly, the formation energy of La_{Cd}^{3+} is the lowest, indicating that the La_{Cd}^{3+} has more stable energetic configuration with local lattice relaxation. To compensate the +3 charge, a $(3/4)V_{Sn}^{4-}$ with opposite charge should be formed in order to keep the local neutrality. In consequence, a charge-compensated complex $4La_{Cd}3V_{Sn}$ is possibly formed. The formation energy is -9.56 eV for $4La_{Cd}3V_{Sn}$.

Calculation results show that if only formation energy is considered, a charge-compensated complex $4La_{Cd}3V_{Sn}$ should be most stable species after La is doped into Cd_2SnO_4 since its energy is the lowest among all possible types of defects. Nevertheless, the rest of defects may also become stable as temperature or the dopant concentration increases, and oxygen vacancies are easily generated in the reducing atmosphere during the preparation of oxides at high temperature. Therefore, it is necessary to investigate the coexistence of La atom and oxygen vacancies in theoretical calculations, the related research on charge compensation in unequal doping has been reported in the literature,[37] so in the next calculation, we only assume one particular type of defect compensation mechanism (*i.e.* localised electronic compensation).

B.   Bader analysis

In order to directly observe the distribution and transfer of electrons in each atom, the Bader charge analysis on the atoms around oxygen vacancy and La doping were investigated. As seen in Fig. 1, the electrotransferred from Cd and Sn atoms to O atoms in V_{O2} and doped systems. Table 1 shows the total charge and charge transfer of the nearest atoms of oxygen vacancy. For
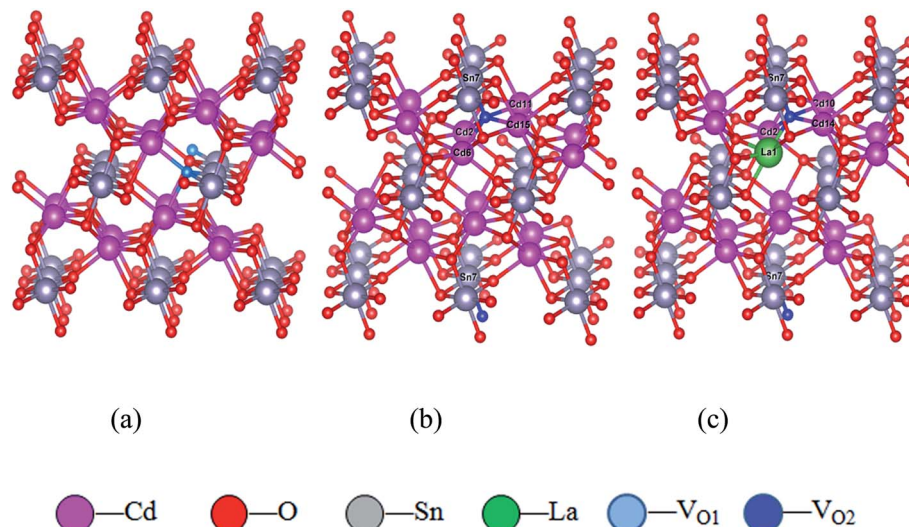
Fig. 1 The supercell models. (a) V_{O1} oxygen vacancy of Cd_2SnO_4 supercell; (b) V_{O2} oxygen vacancy of Cd_2SnO_4 supercell; (c) La-doped Cd_2SnO_4 of V_{O2} oxygen vacancy supercell.

Table 1 The total charge and charge transfer of the nearest atoms of oxygen vacancy

Materials	Atoms	Total Bader charge	Net charge number
CTO	O	7.175	−1.175
	Cd	10.776	1.224
	Sn	11.683	2.317
O-CTO	O	7.198	−1.198
	Cd2	10.952	1.048
	Cd6	10.952	1.048
	Cd11	11.026	0.974
	Cd15	11.000	1.000
	Sn7	11.843	2.157
O-LaCTO	O	7.210	−1.210
	Cd2	10.982	1.018
	Cd10	10.916	1.084
	Cd14	10.901	1.099
	Sn7	12.430	1.570
	La	9.017	1.983

CTO system, O atoms are oxidized and the negative charges in O positions are −1.18. The Cd atoms and Sn atoms are reduced, and the positive charge numbers are 1.22 and 2.32 respectively. Moreover, Cd and Sn atoms are hybridized with O atoms to a certain extent, which makes the outer electrons of Cd and Sn atoms transfer to the O atoms, resulting in Cd and Sn atoms losing electrons and behaving in their reduction state, while O atoms getting electrons with oxidation state.

For the V_{O2} oxygen vacancy of Cd_2SnO_4, the net charge value of the O atom varies little with an average of about −1.20. The number of electrons lost by the Cd atoms is less than that without oxygen vacancies, the transfer electrons numbers approximately equal to 1.048, 1.048, 0.97, 1.00 and the number of electrons of Sn atom lost decreases to 2.16. For the La doped of Cd_2SnO_4, the net charge of O atoms is −1.21, the number of electrons lost by the Cd atoms is 1.018, 1.084, 1.100, the number

of electrons lost by Sn atom is 1.57 and the number of electrons lost by La atom is 1.98. After La doping, the O 2p orbital is hybridized with the La 5d orbital, a large charge transfer of 1.98e is found between La^{3+} and O^{2-} in the La–O interaction. The net charge number of Sn atom is reduced, which indicates that there is a weaker interaction between Sn–O. In general, the charge analysis provides a picture of ionic interactions between the Cd, Sn cations and O anions.

C. Band structure and density of states

Using the GGA+U method, the calculated band gap value of Cd_2SnO_4 is 2.22 eV, which is in good accordance with the experimental band gap of the Cd_2SnO_4 (E_g = 2.3–2.5 eV).[38,39] Thus, the theoretical value agrees well with the experimental data and the selected U values are reasonable. Fig. 2(a) shows the energy band dispersion curves along with six special k points in the Brillouin zone of Cd_2SnO_4. The valence band maximum (VBM) and the conduction band minimum (CBM) are located at Γ point of the Brillouin zone, which indicates that the Cd_2SnO_4 is a direct band-gap semiconductor. Fig. 2(b) and (c) show the band structure of the V_{O2} oxygen vacancy and La doped of Cd_2SnO_4. After the oxygen vacancy is introduced, the Fermi energy level is removed from the top of the valence band, and an impurity energy level caused by an oxygen vacancy in the forbidden zone is close to the Fermi energy level. After the introduction of La doping based on the V_{O2} oxygen vacancy of Cd_2SnO_4, the Fermi energy level enters the conduction band and overlaps with the conduction band which increases the conductivity and the band gap value increases to above 3.0 eV. The impurity energy level caused by oxygen vacancy in the forbidden zone is moved toward the valence band. The extreme values between local energy states above VBM and below CBM are placed in the different points, which means that the valence band and the local O 2p states of electronic transition can directly or indirectly move to the local Cd 4s, Sn 4d and La 5d or
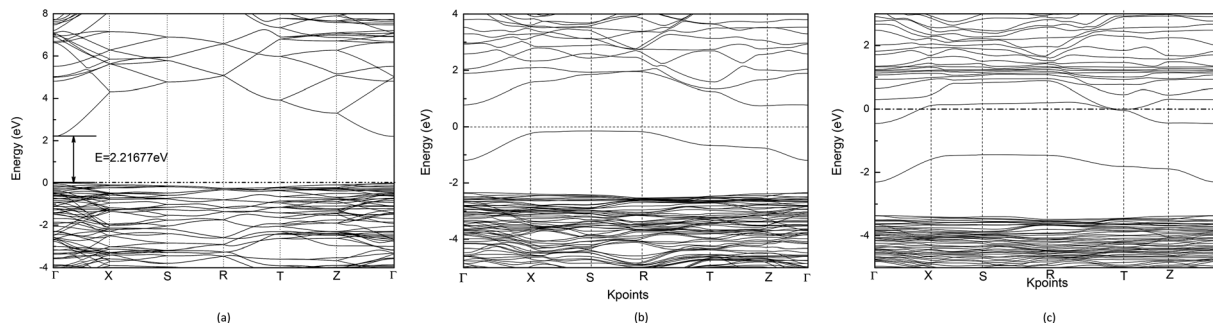
Fig. 2 (a) The band structure of the Cd_2SnO_4 using the GGA+U; (b) the band structure of the V_{O2} oxygen vacancy of Cd_2SnO_4; (c) the band structure of the La doped Cd_2SnO_4 based on the V_{O2} oxygen vacancy.

CBM, and these transitions lead to the change of the optical properties.[40]

The total and partial density of states (DOS) of the perfect Cd_2SnO_4 supercell crystal is presented in Fig. 3. The conduction band is mainly composed of Cd 5s, Sn 5s and Sn 5p orbits, and the overlapping of Cd 4d with O 2p makes up the valence band top. In contrast to Cd_2SnO_4, for V_{O2} oxygen vacancy and La doped of Cd_2SnO_4, some new local energy levels appear in the forbidden zone. The localized energy level of the under and near conduction band is mainly composed of Cd 4s, Sn 4d and La 5d. The above and near valence bands are mainly composed of O 2p states. The local energy level caused by oxygen vacancy is mainly composed of O 2p orbital, with a very small amount of Cd 4s states. The local energy levels caused by La doped oxygen vacancy of Cd_2SnO_4 are mainly composed of O 2p orbitals, with a very small amount of Cd 4s, Sn 4d and La 5d states. The local energy level above the valence band influences the conductivity.[41,42]

D. Optical properties

It is known that the optical properties are determined by the dielectric function $\varepsilon(\omega) = \varepsilon_1(\omega) + i\varepsilon_2(\omega)$, which is mainly contributed from the electronic structures.[43,44] The real part of

Fig. 3 Total and partial density of states of (a) perfect Cd_2SnO_4 and (b) the V_{O2} oxygen vacancy of Cd_2SnO_4 and (c) La-doped Cd_2SnO_4 based on the V_{O2} oxygen vacancy, respectively.

this function, $\varepsilon_1(\omega)$ represents the dispersion of the incident photons by the materials, while the imaginary part $\varepsilon_2(\omega)$ results from the inter-band transition between the occupied state below Fermi level and the unoccupied state above top Fermi level due to the photon absorption. The real part of dielectric function $\varepsilon_1(\omega)$ can be evaluated from imaginary part $\varepsilon_2(\omega)$ through Kramer–Kronig relationship, where $\varepsilon_2(\omega)$ can be treated as detailing the real transitions between occupied and unoccupied electronic states for any materials.[45–48] All other optical constants, such as the absorption coefficient, refractive index and reflectivity can be derived from $\varepsilon_1(\omega)$ and $\varepsilon_2(\omega)$.

Therefore, the imaginary part of the dielectric function $\varepsilon_2(\omega)$ of perfect and V_{O2} oxygen vacancy and La doped of Cd_2SnO_4 is calculated, which is presented in Fig. 4. Considering the tensor nature of the dielectric function, the imaginary parts of the dielectric function are averaged over three polarization vectors (x, y, and z) in our calculations. The peaks of the imaginary part of the dielectric function are related to the electron excitation. From Fig. 4, it can be seen that there are two major peaks located at 7.70 and 10.24 eV for perfect Cd_2SnO_4. Combined with the density of states and electronic band structure analysis, the peaks in perfect Cd_2SnO_4 are mainly owing to the contribution of the direct electron transitions between the O 2p states in the upper valence band and Cd 4d, Sn 4s states in the conduction band. As for V_{O2} oxygen vacancy and La doped of Cd_2SnO_4, the trend is similar with perfect Cd_2SnO_4, the main peaks of the V_{O2} oxygen vacancy of Cd_2SnO_4 locate at 1.80, 2.30, 10.10 and 15.76 eV. In the visible part there are two new peak positions of 1.8 and 2.3 eV, respectively. The first peak mainly comes from within the O 2p local energy states in forbidden band transition to the conduction band; and the second peak is caused by the valence band O 2p state transition to the conduction band. After the doped La atom, the main peaks are located at 2.00, 9.31 and 14.28 eV. The new peak in the visible part of the spectrum is at 2.0 eV, and the peak value is smaller compared with the V_{O2} oxygen vacancy of Cd_2SnO_4. A new peak is also found in the low energy around 0.40 eV for the La-doped is originated by the excitation of O 2p electron from the top of valence band to the impurity energy level which is located at the bottom of the conduction band. Because of the introduction of local energy level, the electron transition between the deep valence band and the conduction band decreases, while the
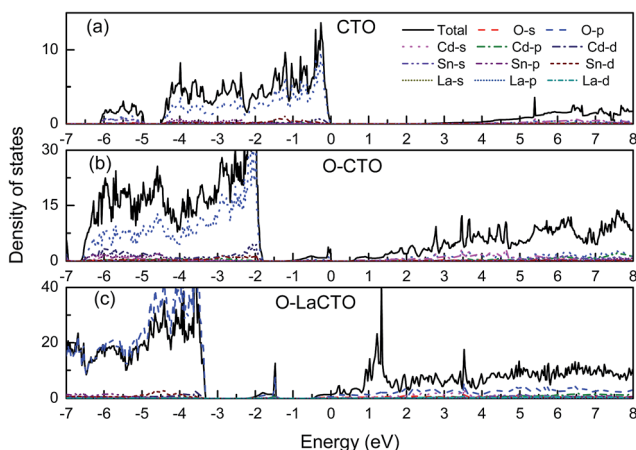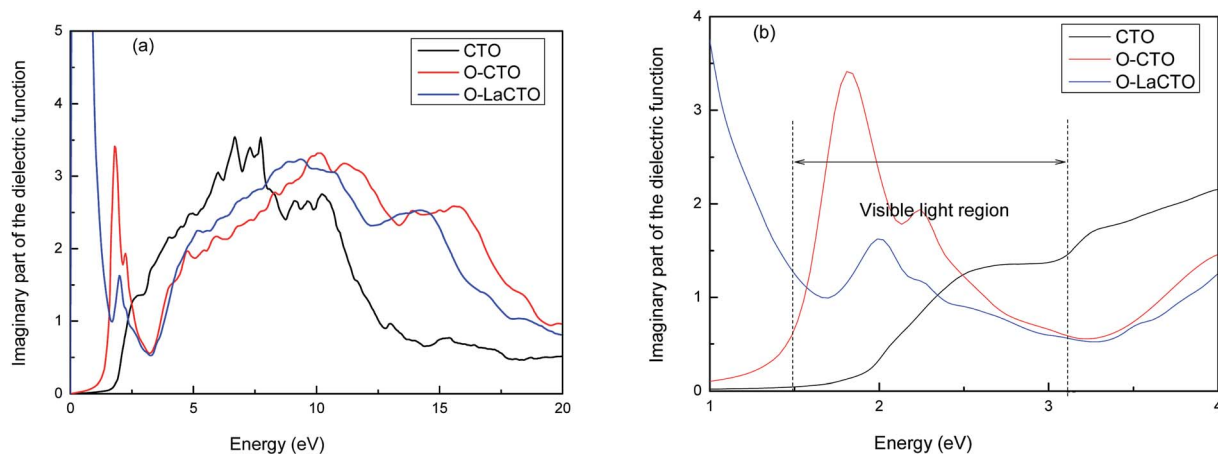
Fig. 4 The imaginary part of the dielectric function of perfect and V_{O2} oxygen vacancy and La doped of Cd_2SnO_4 (a); the visible light region part (b).

electron transition between the local energy level and the conduction band increases.

Transparent conducting materials require low absorption and reflectivity coefficient but high transmittance in the visible light region, so we calculated the absorption, reflectivity, refractive and transmittance. As is shown in Fig. 5(a), the

absorption edge of perfect Cd_2SnO_4 in the visible light region is about 500 nm, which is in conformity with experimental studies, while the optical absorption edge is about 800 nm for V_{O2} oxygen vacancy of Cd_2SnO_4 which is red shifted compare with the perfect Cd_2SnO_4. Oxygen vacancy enables the conduction band to move towards the lower energy, so that the electron
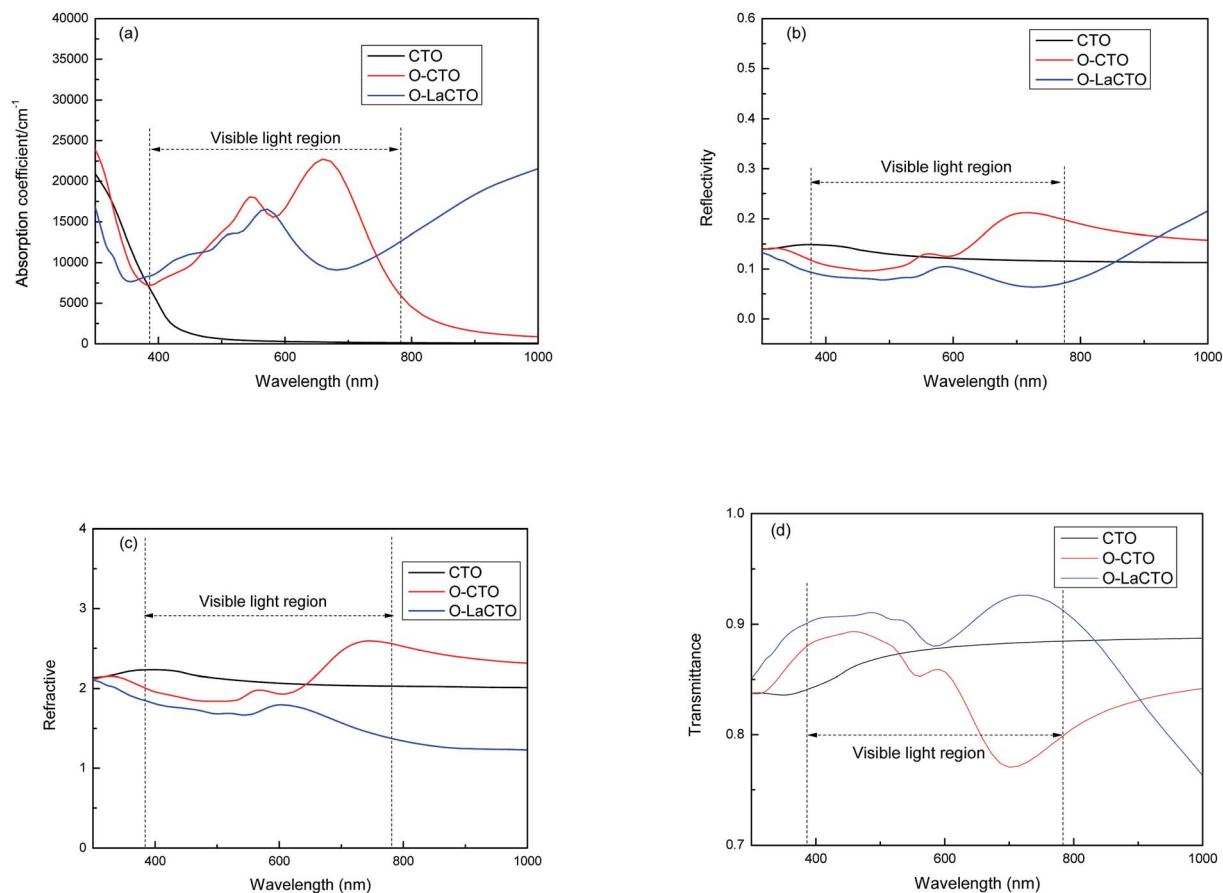

Fig. 5 The variation of the (a) absorption, (b) reflectivity, (c) refractive and (d) transmittance as a function of the wavelength of perfect and V_{O2} oxygen vacancy and La doped of Cd_2SnO_4.

transition can be completed by absorbing only a smaller amount of energy, which eventually leads to the tendency of the absorption spectrum to move to the lower energy (red shift). After the doping of the La atom, the optical absorption coefficient decreases in the visible light region but increases in the infrared region compare with V_{O2} oxygen vacancy of Cd_2SnO_4. The reason why La doped Cd_2SnO_4 increases the absorption in infrared region is that the occupied states close to CBM are shallow donor states, and when the electrons in the local energy level transit to the bottom of the conduction band, these states induce a significant absorption in IR region.

In the visible light region of the spectrum as is shown in Fig. 5(b), it is clear that the perfect Cd_2SnO_4 has a low reflectivity (less than 15%) in the visible and IR regions. However, this reflectivity is decreased in short wavelength (<600 nm) in visible light region and is significantly increased in long wavelength (>600 nm) up to infrared region for V_{O2} oxygen vacancy of Cd_2SnO_4. The reflectivity is the smallest (less than 10%) after doping La atom. As for the refractive index, the trend is similar with reflectivity, as is shown in Fig. 5(c). The refractive index of CTO is about 2.1, and in the short wavelength (<600 nm) for V_{O2} oxygen vacancy of Cd_2SnO_4 the refractive index decreases. After La doping, the refractive index further decreases and the average value is 1.4.

The average transmittance (T) equals to 100% subtract the average reflectance (R) and average absorption (A) ($T = 100\% - R - A$). From Fig. 5(d) it can be concluded that the transmittance of CTO in the visible light region is about 85%. The transmittance of the V_{O2} oxygen vacancy of Cd_2SnO_4 is increased in short wavelength (<600 nm) in visible light region but significantly decreased in long wavelength (>600 nm). After La doped, the transmittance increased to about 90% compared with CTO and V_{O2} oxygen vacancy of Cd_2SnO_4. It is indicated that the presence of oxygen vacancies is not conducive to the enhancement of the optical properties of transparent conducting materials. Therefore, it is necessary to control the occurrence of oxygen vacancies in the experiment and increase the transmittance by doping different atoms.

IV. Conclusions

The electronic structure and optical properties of oxygen vacancy and La-doped Cd_2SnO_4 were calculated using the GGA+U method based on the first principles calculations. It was found that the impurity levels appeared in the forbidden band for Cd_2SnO_4 with oxygen vacancies, and the impurity levels caused by oxygen vacancy mainly were composed by O 2p orbital, mixed with a small amount of Cd 4s orbital. After La doping, the Fermi level entered the conduction band, overlapping with the conduction band and the conductivity being improved. The results of Bader charge analysis showed that there was a slightly stronger interaction between La and O atoms but a weaker interaction between Sn and O atoms after La atom doping. The results of optical performance analysis showed that the transmittance caused by oxygen vacancy increased in short wavelength but decreased in long wavelength up to infrared region, and the transmittance of La atom doping

increased in visible light region compared with Cd_2SnO_4. Therefore, it was necessary to increase the transmittance by doping different atoms in the experiment.

Conflicts of interest

There are no conflicts to declare.

Acknowledgements

References

1 D. S. Ginley and C. Bright, *MRS Bull.*, 2000, **25**, 15–18.

2 T. Minami, *MRS Bull.*, 2000, **25**, 38–44.

3 T. J. Coutts, D. L. Young and X. N. Li, *MRS Bull.*, 2000, **25**, 58–65.

4 A. J. Smith, *Acta Crystallogr.*, 1960, **13**, 749–752.

5 A. J. Nozik, *Phys. Rev. B: Condens. Matter Mater. Phys.*, 1972, **6**, 453–459.

6 X. Wu, R. Ribelin, R. G. Dhere, D. S. Albin, T. A. Gessert, S. Asher, D. H. Levi, A. Mason, H. R. Moutinho and P. Sheldon, *Proceedings of the 28th IEEE Photovoltaic Specialists Conference*, IEEE, 2000, pp. 470–474.

7 X. Z. Wu, *Sol. Energy*, 2004, **77**, 803–814.

8 A. W. Metz, M. A. Lane, C. R. Kannewurt, K. R. Poeppelmeier and T. J. Marks, *Chem. Vap. Deposition*, 2004, **6**, 297–300.

9 R. A. Ismail, S. A. Tawfiq, R. Hababa, R. S. Sabry and O. A. Abdulraza, *e-J. Surf. Sci. Nanotechnol.*, 2007, **5**, 152–154.

10 R. Kumaravel, V. Krishnakumar, V. Gokulakrishnan, K. Ramamurthi and K. Jeganathan, *Thin Solid Films*, 2010, **518**, 2271–2274.

11 C. J. D. Godines, C. G. T. Castanedo, R. C. Pérez, G. T. Delgado and O. Z. Ángel, *Sol. Energy Mater. Sol. Cells*, 2014, **128**, 150–155.

12 B. Schumm, P. Wollmann, J. Fritsch, J. Grothe and S. Kaskel, *J. Mater. Chem.*, 2011, **21**, 10697–10704.

13 H. M. Ali, H. A. Mohamed, M. M. Wakkad and M. F. Hasaneen, *Jpn. J. Appl. Phys.*, 2009, **48**, 041101.

14 N. Miyata, K. Miyake and S. Nao, *Thin Solid Films*, 1979, **58**, 385–389.

15 N. Miyata, K. Miyake and Y. Yamaguchi, *Appl. Phys. Lett.*, 1980, **37**, 180–182.

16 A. M. Al-Baradi, M. M. El-Nahass, M. M. A. El-Raheem, A. A. Atta and A. M. Hassanien, *Radiat. Phys. Chem.*, 2014, **103**, 227–233.

17 M. M. El-Nahass, A. A. Atta, M. M. A. El-Raheem and A. M. Hassanien, *J. Alloys Compd.*, 2014, **585**, 1–6.

18 R. Mamazza Jr, D. L. Morel and C. S. Ferekides, *Thin Solid Films*, 2005, **484**, 26–33.

19 K. Jeyadheepan, M. Thamilselvan, K. Kim, J. Yi and C. Sanjeeviraja, *J. Alloys Compd.*, 2015, **620**, 185–191.

20 S. M. Al-Sofiany and H. E. Hassan, *J. Alloys Compd.*, 2015, **651**, 149–156.

21 S. H. Lee, E. W. Lee, S. Y. Park and C. W. Jeon, *Mol. Cryst. Liq. Cryst.*, 2010, **532**, 106–111.

22 D. L. Peng, S. R. Jiang and W. L. Wang, *Chin. Phys. Lett.*, 1993, **10**, 189–192.

23 W. L. Wang, K. J. Liao, C. Z. Cai, G. B. Liu and Y. Ma, *Surf. Coat. Technol.*, 2003, **167**, 284–287.

24 S. Y. Sun, J. L. Huang and D. F. Lii, *J. Mater. Res.*, 2005, **20**, 2030–2037.

25 T. J. Coutts, D. L. Young, X. Li and X. Wu, *J. Vac. Sci. Technol., A*, 2000, **18**, 2646–2660.

26 T. Stapiński, E. Leja and T. Pisarkiewicz, *J. Phys. D: Appl. Phys.*, 1984, **17**, 407–413.

27 G. Haacke, W. E. Mealmaker and L. A. Siegel, *Thin Solid Films*, 1978, **55**, 67–81.

28 G. Kresse and J. Furthmuller, *Phys. Rev. B: Condens. Matter Mater. Phys.*, 1996, **54**, 11169–11186.

29 G. Kresse and J. Furthmuller, *Comput. Mater. Sci.*, 1996, **6**, 15–50.

30 J. P. Perdew, K. Burke and M. Ernzerhof, *Phys. Rev. Lett.*, 1996, **77**, 3865–3868.

31 G. Kresse and D. Joubert, *Phys. Rev. B: Condens. Matter Mater. Phys.*, 1999, **59**, 1758–1775.

32 H. J. Monkhorst and J. D. Pack, *Phys. Rev. B: Condens. Matter Mater. Phys.*, 1976, **13**, 5188–5192.

33 X. G. Ma, Y. Wu, Y. H. Lv and Y. F. Zhu, *J. Phys. Chem. C*, 2013, **117**, 26029–26039.

34 S. J. Wang, X. B. Shi and J. M. Li, *RSC Adv.*, 2016, **6**, 107865–107870.

35 X. L. Huang, J. Lv, Z. S. Li and Z. G. Zhou, *ChemInform*, 2010, **41**, 341–344.

36 C. G. Van de Walle and J. Neugebauer, *J. Appl. Phys.*, 2004, **95**, 3851–3879.

37 J. Han, L. J. Li, M. Y. Peng, B. L. Huang, F. J. Pan, F. W. Kang, L. Y. Li, J. Wang and B. F. Lei, *Chem. Mater.*, 2017, **29**, 8412–8424.

38 G. M. Zhang, Z. Y. Fu, Y. C. Wang, H. Wang and Z. Xie, *RSC Adv.*, 2015, **5**, 83922–83930.

39 S. Dinesh, M. Anandan, V. K. Premkumar, S. Barathan, G. Sivakumar and N. Anandhan, *Mater. Sci. Eng., B*, 2016, **214**, 37–45.

40 D. Steiauf, J. L. Lyons, A. Janotti and C. G. Van de Walle, *APL Mater.*, 2014, **2**, 52.

41 A. Janotti and C. G. Van de Walle, *Appl. Phys. Lett.*, 2005, **87**, 122102.

42 M. Choi, A. Janotti and C. G. Van de Walle, *J. Appl. Phys.*, 2013, **113**, 044501.

43 A. Slassi, *Optik*, 2015, **126**, 4751–4756.

44 J. F. Guo, W. Zhou, P. F. Xing, P. Q. Yu, Q. G. Song and P. Wu, *Solid State Commun.*, 2012, **152**, 924–928.

45 S. A. Kelkar, P. A. Shaikh, P. Pachfule and S. B. Ogale, *Energy Environ. Sci.*, 2012, **5**, 5681–5685.

46 A. Slassi, S. Naji, A. Benyoussef, M. Hamedoun and A. El Kenz, *J. Alloys Compd.*, 2014, **605**, 118–123.

47 R. S. Zhang, Y. Liu, Q. Gao, F. Teng, C. L. Song, W. Wang and G. R. Han, *J. Alloys Compd.*, 2011, **509**, 9178–9182.

48 H. Y. Yan, Y. R. Guo, Q. G. Song and Y. F. Chen, *Phys. B*, 2014, **434**, 181–184.